Heliyon

Received:
9 October 2018
Revised:
20 December 2018
Accepted:
11 February 2019

Cite as: Suebchat Kanthiya, Niti Mangkhemthong, Christopher K. Morley. Structural interpretation of Mae Suai Basin, Chiang Rai Province, based on gravity data analysis and modelling. Heliyon 5 (2019) e01232. doi: 10.1016/j.heliyon.2019.e01232

Structural interpretation of Mae Suai Basin, Chiang Rai Province, based on gravity data analysis and modelling

Suebchat Kanthiya, Niti Mangkhemthong*, Christopher K. Morley

Department of Geological Sciences, Chiang Mai University, Chiang Mai, 50200, Thailand

* Corresponding author.

E-mail address: niti.ace@gmail.com (N. Mangkhemthong).

Abstract

The Mae Suai Basin, an intermountain basin in northern Thailand, became an area of interest in 2014 following the M6.1 earthquake that reactivated the ENE-WSW trending Mae Loa Fault. This fault is associated with the Cenozoic rifting. Terrestrial gravity modelling is a suitable method to visualize subsurface geometry and understand its structural control related to the recent earthquakes. Six hundred twenty-seven terrestrial gravity stations with a spacing of ~500 m were collected; standard gravity correction methods were applied with a density reduction of 2.67 g/cm^3 to produce the residual Complete Bouguer anomaly (CBA). The residual CBA map reveals a NNE-SSW striking basin, showing gravity lows are located within the basin. The gravity highs cover regions of Triassic granite intrusions to the west and Silurian-Devonian metasedimentary and Carboniferous sedimentary basements to the east. Structural edge detections and basin depth estimates indicate the main fault lineaments lie ENE-SWS and NNE-SSW striking along the eastern and northern margins respectively. These faults may act as splay faults of the active sinistral Mae Loa fault. The gravity models suggest that the Mae Suai Basin is an asymmetrical half-graben with a maximum depth of ~770 m and a range of basin sediments from 1.9 to 2.3 g/cm^3. The depocentre is located near the eastern boundary faults. The structural patterns present the rifting has formed within an extensional transfer zone that

https://doi.org/10.1016/j.heliyon.2019.e01232

relates to a releasing bend fault in NNE-SSW trend, linked by the sinistral Mae Loa Fault in NE-SW trend. The E-W maximum of extension in the transfer zone is formed under the activation of the major Cenozoic strike-slip faults in Northern Thailand.

Keywords: Geology, Geophysics

1. Introduction

The Cenozoic rift basins of Northern Thailand (Fig. 1) are economically important in providing fuel resources such as petroleum coal, and oil shale (e. g. Morley and Racey, 2011). The basins also contain a record of Cenozoic tectonic events and stress variations that show how extensional rift basins have formed (e. g. Morley et al., 2011; Morley, 2009; Uttamo et al., 2003a) and related to regional escape tectonics related to the Himalaya collision and recent seismology. However, despite seismic, borehole, and open deep cast mining data being available for some large basins, our understanding is far from comprehensive, with the geology of many small basins being unknown or limited to terrestrial geophysical surveys (e. g.

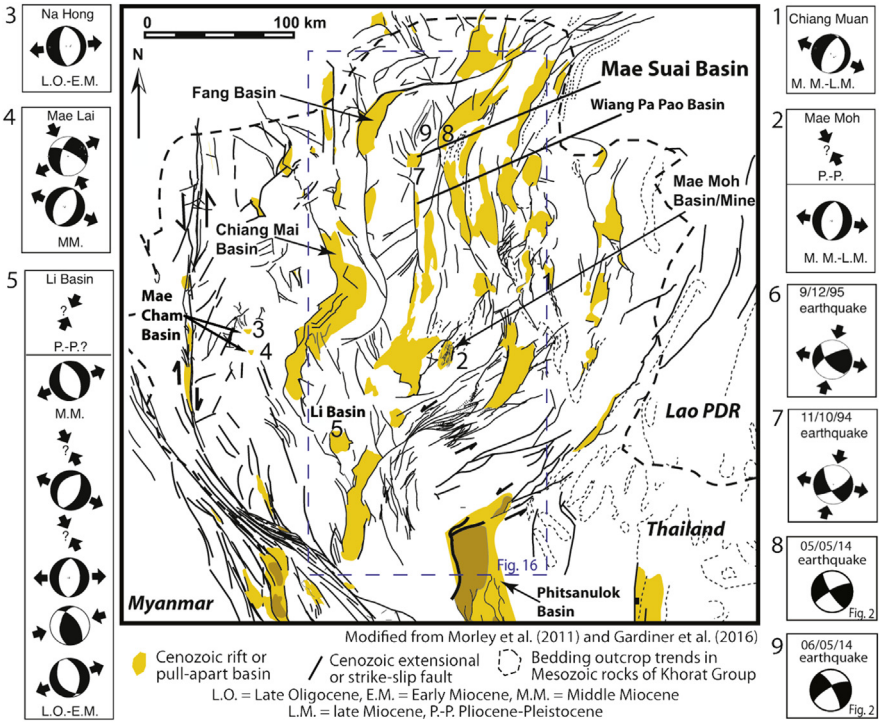

Fig. 1. Regional map of Central and Northern Thailand, showing the locations of major Cenozoic faults and sedimentary basins with moment tensor analyses of recent earthquakes (modified from Gardiner et al., 2016; Morley et al., 2011).

https://doi.org/10.1016/j.heliyon.2019.e01232

Milsom, 2011; Wattananikorn et al., 1995). Some small basins are associated with significant recent earthquakes.

On 5 May 2014 at 11:08:43 UTC, a M6.1 earthquake, the Mae Lao earthquake, the largest earthquake magnitude recorded in Thailand this decade, occurred at ~6 km depth in northern Thailand (U.S. Geological Survey: USGS, 2014) with an epicenter located at latitude 19.69° N and longitude 99.69° E in Pan District. Pananont et al. (2017) suggested the main shock was generated on NNW-SSE trending Phayao Fault Zone, with dominantly right lateral strike-slip motion (Fig. 2b). Approximately 1,000 aftershocks were recorded in the months following the main shock with epicentres covering a large area of southern and western Chiang Rai Province (Fig. 2a). One of the earthquake series was the M5.3 located at latitude 19.70° N and longitude 99.53° E in the northern Mae Suai District. Focal mechanism solutions indicate an ENE-WSW trending fault with a strike-slip movement sense caused the aftershock series (Fig. 2b) (Noisagool et al., 2016; Pananont et al., 2017). Earthquake locations and vibrations were thought to be related regarding orientation and behaviour to the movement on the Mae Lao Fault Segment of the Phayao Fault Zone (Figs. 1 and 2a), here called the Mae Lao Fault (MLF) (DMR, 2007; Noisagool et al., 2016). Therefore, this recently significant earthquake event leads the Mae Suai Basin (MSB) to be an area of interest for surface and subsurface investigations.

The geometry of the late Cenozoic MSB (Fig. 1), is poorly defined due to the absence of surface exposures, and limited subsurface control by shallow (<100 m) resistivity data provided by the Department of Mineral Resources, DMR (2014) and Department of Groundwater Resources, DGR (2009). Based on an

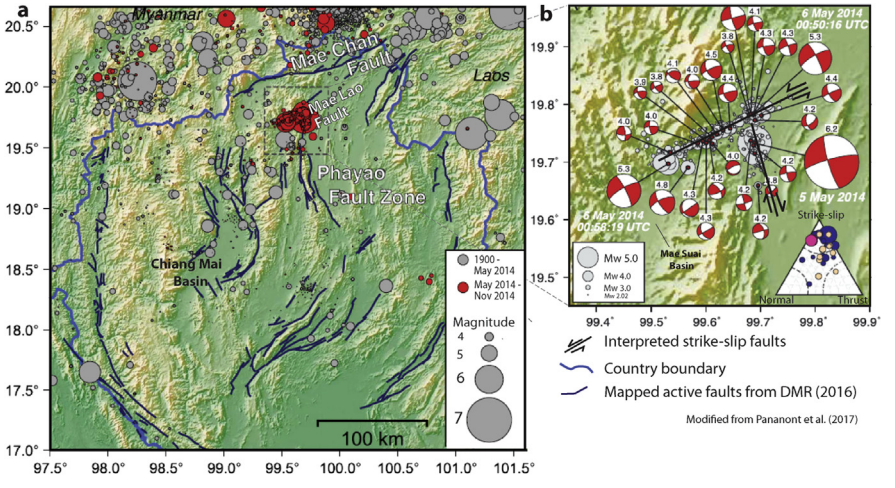

Fig. 2. a) Seismicity of Northern Thailand and surrounding regions showing earthquakes generated before the 2014 Earthquake main shock (grey circles), and the 2014 main shock and seismicity after that time up to late 2015 (red circles) (modified from Pananont et al., 2017). b) The Regional moment tensor solutions showed focal mechanisms for 27 Earthquakes (Fig. 2a, a dashed rectangle). The solutions suggest interpretations of ENE-WSW sinistral and NNW − SSE dextral movements during the shocks.

https://doi.org/10.1016/j.heliyon.2019.e01232

interpretation of surface data Uttamo et al. (2003a) interpreted the MSB as an extensional basin (Fig. 1). The associated left-lateral strike-slip MLF to the northeast of the Mae Suai area may have been activated during the high magnitude earthquake in 2014 (USGS, 2014). Consequently, understanding the basin geometry and related fault geometries has become important for understanding the context of seismicity in the area. A terrestrial gravity investigation is a standard initial method used to determine the geometry of sedimentary basins to understand the subsurface geometry and structure in the basin, where density lows are related to the basin fill, and density highs are present over the surrounding basement terrain.

Gravity measurements can utilize variations in the gravitational field where density contrasts are present, particularly lateral variations associated with geology or structure of subsurface (Hinze et al., 2012). Subsurface geometry is obtained based on the Earth's gravitational field variations related to the source body (Kearey et al., 2002). Gravity data over areas that display a younger, less dense sedimentary section juxtaposed with older, denser rock units can be used to define the nature of the basin geometry, and its contacts with adjacent basement rocks. The gravitational potential field technique has been widely used for exploration at the basin and regional scales. The gravity method is essentially an enhancement of the geological interpretation which can reasonably solve geological and structural problems in areas of limited exposures and subsurface information, such as intermountain basin areas in northern Thailand.

This study reveals the subsurface geometry of the MSB using a ground-based gravity survey that covers the entire basin. Numerical geophysical filtering techniques were applied to the gravity data to enable the production of 2-D cross-section models of the basin morphology (Fig. 3). Gravity data filtering and modelling were processed using the Geosoft Oasis montaj® software package. The processing aimed to detect the basin boundaries and estimate the basin depth. Geophysical processing techniques of the total horizontal derivative, the Euler deconvolution, the second order (2^{nd}) of horizontal derivative, radial spectral analysis, and the depth to basement were applied to constrain the basin boundaries and for fault detections. Six 2-D forward models were generated and then interpolated to make a 3-D reference model, and density inversion models of the MSB (Fig. 3). This approach to 3-D modelling can produce a more realistic subsurface geometry because the reference model is controlled by the user and is based upon a combination of geological and geophysical data (Blaikie et al., 2014). We also compared our gravity modelling results to geological information to help confirm the MSB's subsurface structures.

2. Geological setting

Cenozoic tectonics of the northern Thailand intermountain province is dominated by the opening of N-S to NNE-SSW trending rift basins (Fig. 1), that are commonly

https://doi.org/10.1016/j.heliyon.2019.e01232

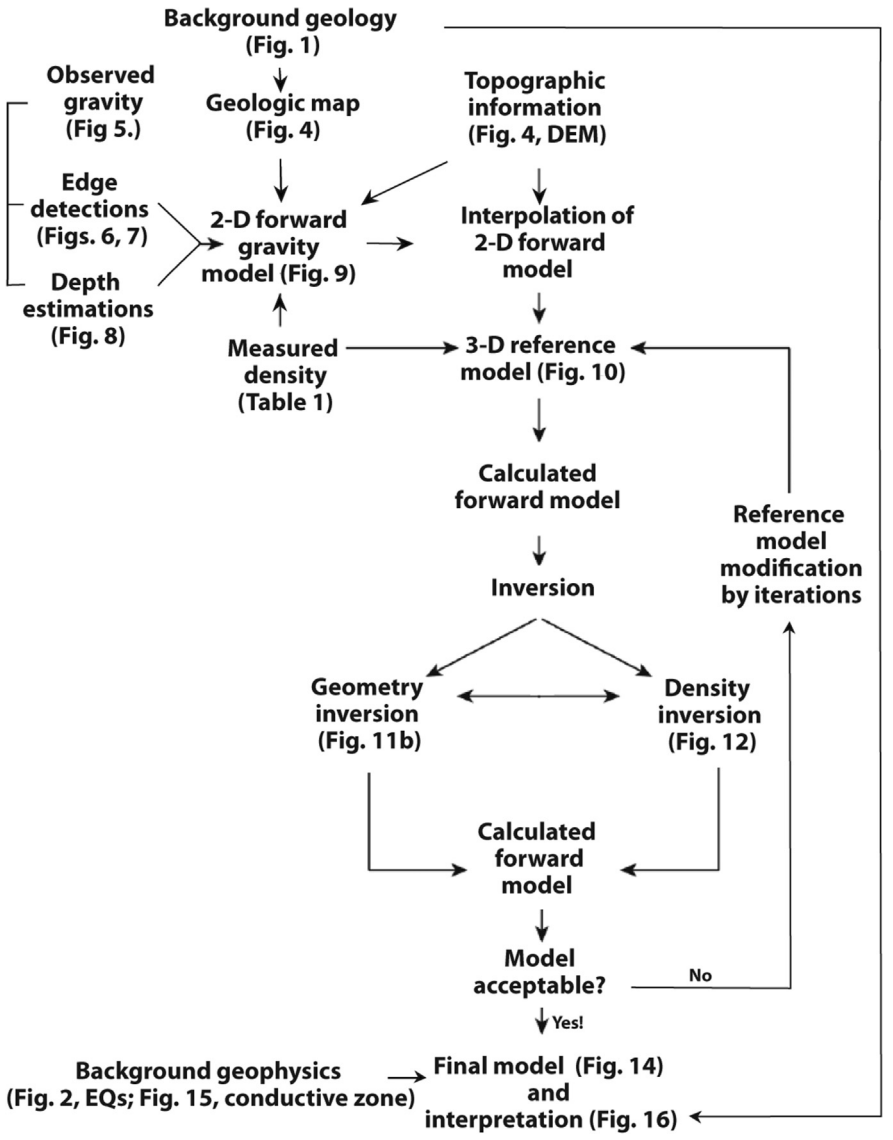

Fig. 3. A workflow diagram for 2-D forward and 3-D inversion gravity modelling (modified from McLean et al., 2008; Skalbeck et al., 2014).

bounded by NE, ENE, and NW-trending of strike-slip faults (Morley, 2007; Rhodes et al., 2003). The Mae Suai Basin (MSB) is one of around forty intermountain basins in the Basin and Range Province of Northern Thailand. The basins typically exhibit half graben geometries and are less than 3 km thick (Morley and Racey, 2011). The rift basins of Thailand have formed under the E-W extensional regime that is related to subduction activity of the India-Eurasian collision in early Eocene (50 Ma) (Morley, 2009). The rift basins grade westwards and northwards into regimes that are strike-slip dominated. In addition to the spatial variations in structural style, there are temporal changes as well. In Northern Thailand the Miocene extensional basins are overprinted by latest Miocene-Recent, strike-slip dominated deformation as the

https://doi.org/10.1016/j.heliyon.2019.e01232

effects of Himalayan-related deformation have propagated to the south with time (Morley, 2007; Morley et al., 2011).

The ENE-WSW to NNE-SSW trending faults in Northern Thailand, such as the Mae Chan Fault, show a variety of characteristics (Morley, 2007) including 1) an oblique sinistral extensional offset appropriate for E-W extension during the Late Oligocene-Miocene and (2) episodic reversal to dextral displacement during periods of basin inversion (particularly around the Miocene-Pliocene boundary). Some of the characteristics of inversion are folding structures, uplift of rifting basins, and unconformities (Morley, 2001; Morley et al., 2000). Multiple episodes of inversion alternating with extension have occurred in some basins (Morley et al., 2000). These observations differ from the regional dextral (older) to sinistral (younger) switch models for NE-SW to ENE-WSW strike-slip faults seen further north and west in Lao PDR, Myanmar, and Yunnan (Lacassin et al., 1997).

The MSB basin is 30 km long and 60 km wide (DMR, 2007; Uttamo et al., 2003a, Fig. 4). The low-relief region of the basin area is mostly filled with Tertiary and Quaternary accumulations in an intermountain basin. The basin sediments were locally derived from the topographically high terrains of the granite pluton to the west and metasedimentary-sedimentary assemblages to the east. The Silurian-Devonian age unit described by Wongwanich and Boucot (2011) is the oldest mapped rock unit in the area. The low-grade metamorphic rocks extend between Chiang Mai and Chiang Rai and comprise of schist, phyllite, and chert. These Silurian-Devonian metamorphic rocks are named the Mae Ko Complex. Piyasin (1972) estimated the thickness of this basement at 1500 m. The Carboniferous section comprises sandstone, shale, and limestone that is exposed in small patches in the western region. The unit was mapped as unconformably overlying the Silurian-Devonian section (Barr et al., 1990). The Carboniferous clastic rocks were assigned to the Mae Tha Formation, which has a thickness of about 400 m (Bunopas, 1981). The Triassic granite intrusion located in the western part of the study area is interpreted as the youngest basement unit and is called the Fang Batholith (Cobbing, 2011, Fig. 4). The MSB is considered to be a half-graben shape (Uttamo et al., 2003a). The satellite images analysis and a structural geology interpretation from Uttamo et al. (2003b) and Khamphira (2016) have identified two main fault systems that lie along the eastern and northeastern parts of the basin.

Two major fault zones consisting of the Mae Chan and Phayao Fault Zones lie close to the locality of the MSB (DMR, 2001) (Fig. 2a). The ENE-WSW trending Mae Chan Fault Zone is 150 km long and displays sinistral movement (Morley, 2007). This fault terminates at the northern tip of the Fang Basin (Uttamo et al., 2003a) and is associated with the development of the Fang Basin (Morley, 2007). The Phayao Fault Zone trends NNW-SSE is 35 km long and acts as an oblique-slip fault with dextral and normal motion, the fault runs parallel to the western margin of

https://doi.org/10.1016/j.heliyon.2019.e01232

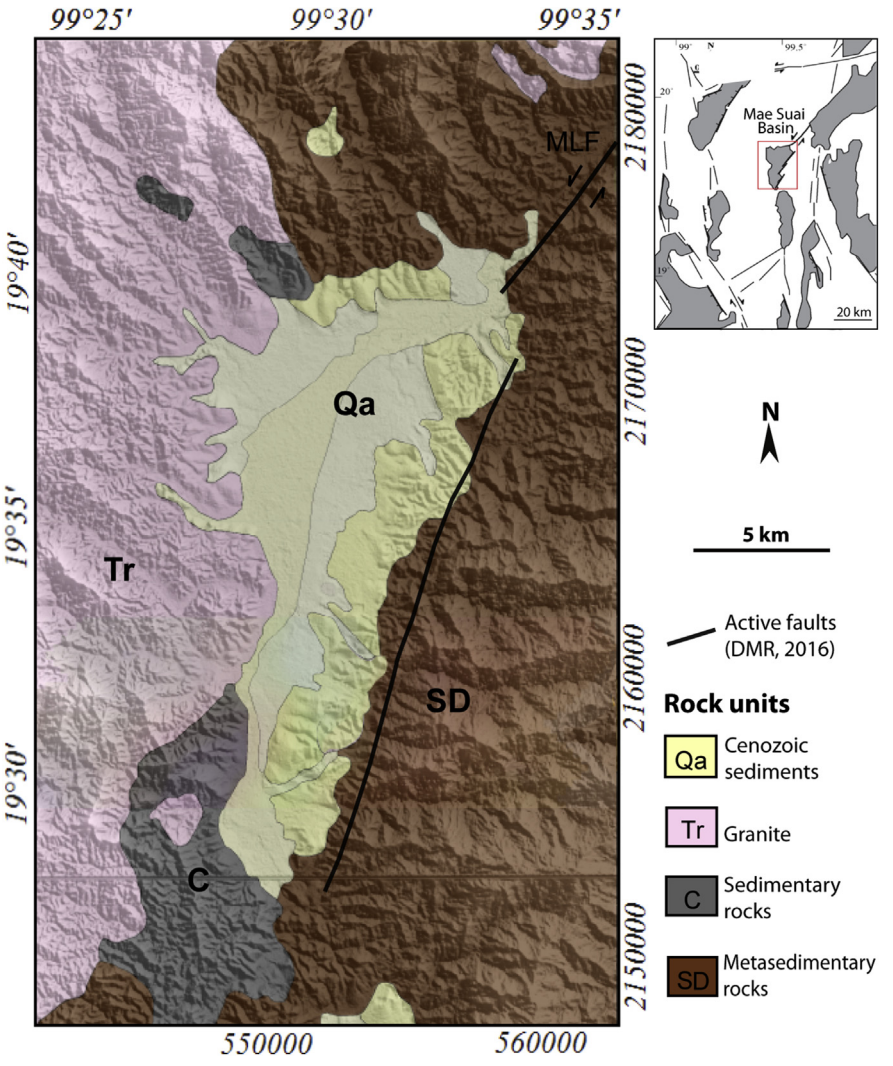

Fig. 4. Simplified geologic map of Mae Suai Basin and surrounding basement rock terranes (modified from DMR, 2007). Solids black lines indicate surface faults mapped by DMR (2016).

Southern Chiang Rai Basin. Interacting with the Phayao Fault Zone is the ENE-WSW striking, sinistral Mae Lao Fault which affects the northeastern and northern margins of the MSB (Fig. 4).

3. Methods

3.1. Gravity data collection and reduction

The gravity data collected for this study covers an area of 600 km^2 in the Mae Suai District. A total of 627 gravity data were acquired with an observation spacing of around 500 m (Appendix A). A CG-3 Scintrex Autograv gravity meter, with data survey accuracy of 0.01 mGal, was used for the survey (Fig. 5). A Topcon

https://doi.org/10.1016/j.heliyon.2019.e01232

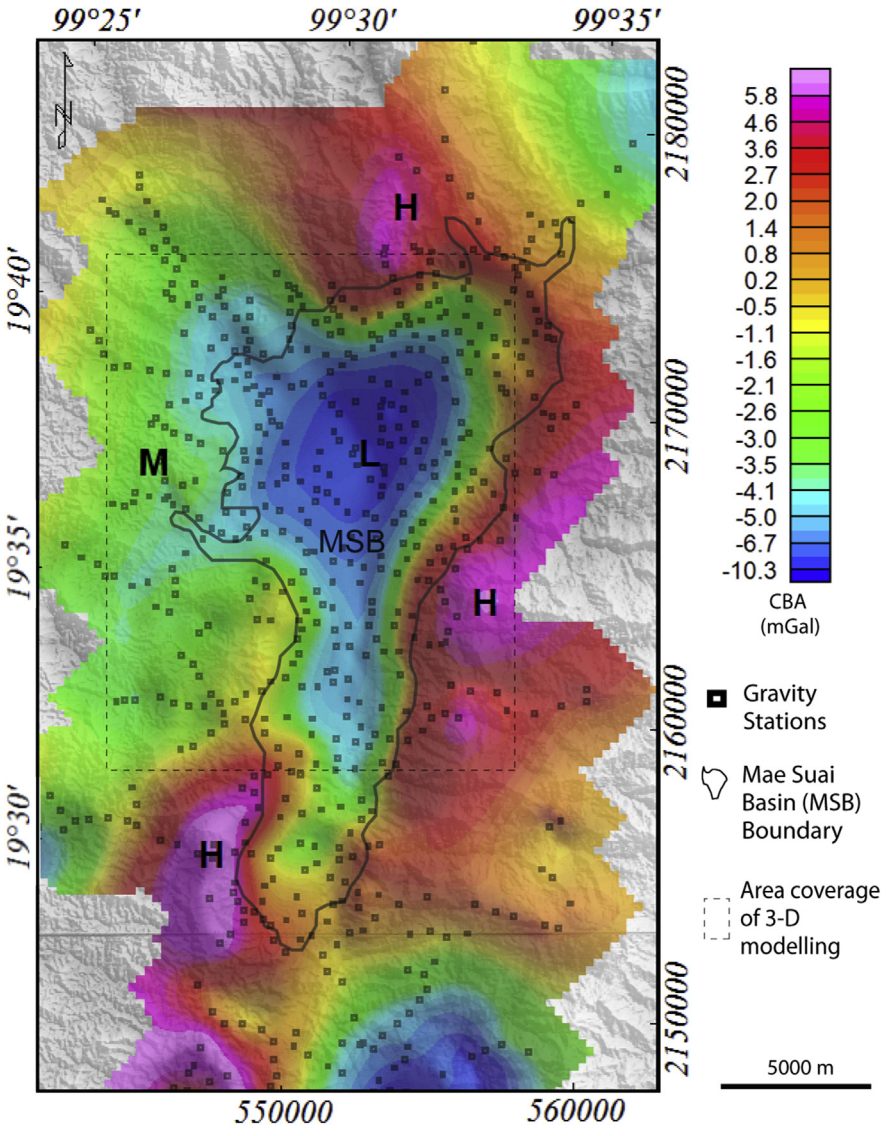

Fig. 5. Residual Complete Bouguer Anomaly map of Mae Suai Basin overlying a Digital Elevation Model data. Gravity variations of lows, moderates, and highs are labelled as L, M, and H, respectively.

differential GPS was used to control the vertical elevations and has a post-processing accuracy of less than 0.2 m. The collected gravity data contained temporal variations ranging around 0.05−0.2 mGal per a 3−5-hour survey loop due to the Earth tidal and measurement drift that had to be linearly eliminated (Robinson and Crouch, 1998). The Latitude Correction was applied to minimize the gravity effect of the Earth's elliptical shape and rotation. The 1967 International Gravity Formula (IGF67) for datum reference was used for Free-air and Bouguer slab corrections where an applied reduction in density of 2.67 g/cm^3 was used. Mass effects due to topography surrounding the observation site have to be minimized. The Terrain correction method described by Whitehead and Musselman (2006) added to the

https://doi.org/10.1016/j.heliyon.2019.e01232

SBA yields the Complete Bouguer Anomaly (CBA; supplementary material). The trend analysis has to be processed to ideally eliminate the long wavelength gravity anomaly generated from deep regions. Therefore, the residual CBA (Fig. 5) of basin and basement sources has been produced for geophysical interpretation and analysis using the minimum curvature gridding method with a grid cell size of 270 m. The Geosoft Oasis montaj® software was used to produce gravity anomaly maps.

3.2. Gravity data processing

The structural boundaries of the Mae Suai Basin (MSB) in the 2-D modelling process are constrained using the edge detection techniques for gravitational field data consisting of the total horizontal derivative, the Euler deconvolution, and the 2^{nd} horizontal derivative. The horizontal derivative method produces a maximum ridge of anomaly gradients over the contacts between different densities among subsurface rock units that are caused by features such as stratigraphic or structural contacts which juxtapose units of different densities (Whitehead and Musselman, 2006). We applied the Euler Deconvolution technique of three orthogonal gradients along x, y, and z-axes of potential field to integrally estimate subsurface locations in both horizontal and vertical (depth) dimensions of an anomaly source (Reid et al., 1990). In practice, Structure Index and Window Size are run together with gradient data in the least-square inversion to deconvolve the subsurface location (Hinze et al., 2012). Note that appropriate parameters of Euler calculation for ideal fault contacts were set at Structure Index of 0 and Window Size of 15 (Whitehead and Musselman, 2006). Moreover, determination of fault trends associated with the interpreted faults of previous literature (e. g. DMR, 2016; Morley, 2007) could be achieved by a zero trending of the 2^{nd} horizontal derivative method in the appropriated gradient directions of azimuths 135^{o} and 100^{o} (Whitehead and Musselman, 2006) perpendicular to the structural target of fault strikes. These possible fault lineaments can be identified and mapped.

The radial spectral analysis method is useful in determining an average basin depth based on a statistical ensemble of potential anomaly sources (Spector and Grant, 1970). The graph of wavenumber with the change of the spectral decay rates (slope) against the power of a signal's amplitude values was extracted and grouped as slopes of a basement, sediment basin, and surface noise anomaly sources. Therefore, the average radial spectrum of basin sediments can be directly identified. We also applied a semi-automatic source detection using the technique of analytic signal amplitude called the Pdepth method to yield subsurface depth constraints along the 2-D profiling data. The depth to basement solutions are calculated by discrete depth solutions of assumed structural contacts (Nabighian, 1972; Thurston and Smith, 1997; Whitehead and Musselman, 2006) and represented as clustered points of the structural contact locations. The used parameters for computing discrete depth

https://doi.org/10.1016/j.heliyon.2019.e01232

solutions by moving spatial window were set between 500 m to 2000 m for the minimum and maximum window operator length, respectively, with a 100 m expansion increment.

3.3. The 2-D forward gravity modelling

We used the GM-SYS Profile Modelling Module® to produce 2-D forward models of the geologic structures over the study area to reveal the subsurface geometry information based on the Talwani et al. (1959) method. Six profiles of 2-D gravity models were constructed extending about 10 km in a NW-SW direction perpendicular to a basin orientation. We modelled structures to a depth of ~2 km and assumed homogeneous bodies extending orthogonally to the profiles to distances effectively of infinity (±30,000 km). Forward modelling was conducted to minimize gravity misfits between observed and calculated gravity anomaly data and to define the most reasonable geological model. The non-uniqueness limitation of gravity modelling and the absence of other subsurface data means that all available surface data such as topography, depth, body shape, density, and subsurface data from the integration of earlier gravity data analysis are considered as a data constraints for the forward model. The published geologic map from DMR (2007) was used for geologic contacts. A digital elevation model dataset with the 30-metre resolution was used for topographic constraints (Figs. 3 and 4).

Appropriate densities from 36 rock samples and standard rock's density information of basement rocks (e. g. Telford et al., 1990; Wattananikorn et al., 1995) were used as modelling parameters (Table 1). We modelled density parameter inputs as a homogeneous unit with a uniform density; although in reality, the units are heterogeneous because of different sedimentation ages and facies in layered sediment and rock units and multiple intrusion phases in igneous units. Four density blocks were modelled comprising: 1) Silurian-Devonian metasedimentary rocks with a density of 2.68 g/cm^3, 2) Carboniferous sedimentary rocks with a density of 2.55 g/cm^3,

Table 1. Rock density estimations for 2-D forward gravity modelling.

Rock units	Rock density (g/cm^3)		
	Density estimation from rock samples	Telford et al. (1990)	Wattananikorn et al. (1995)
Triassic granite rocks (5 samples)	2.64 ± 0.03[#]	2.64	2.62
Silurian-Devonian metasedimentary rocks (5 samples)	2.68 ± 0.04[#]	2.71	-
Carboniferous Sedimentary rocks (4 samples)	2.55 ± 0.07[#]	2.35	-
Cenozoic Sediments	-	2.2[#]	2.15 to 2.3

[#] densities were used for 2-D forward gravity modelling.

https://doi.org/10.1016/j.heliyon.2019.e01232

3) Triassic granitic rocks with a density of 2.64 g/cm^3, and 4) Cenozoic sediments with a density of 2.20 g/cm^3 referred from Telford et al. (1990). Note that these pseudo-geological models were created with an assumption that the Earth has no curvature and the model can be extended to an infinite distance to unconsidered lateral edge effects of the density body (Talwani and Heirtzler, 1964).

The interpretations of pseudo-geological models yield non-unique solutions between rock density and a modelled basin geometry (Kearey et al., 2002). Several model members can be constructed to fit the observed gravity data. The most geologically reasonable models that exhibit the least complexities in geology and structure with the minimum misfits were selected for the final models. The greater misfits appear along the two sides the models due to less gravity data constraints beyond. A half mGal is an accepted root mean square misfit error for the pseudo-geological modelling.

3.4. The 3-D inverse gravity modelling

We inverted residual CBA data to develop a structural surface model of the base of the basin using the GM-SYS 3D Modelling Module® based on the initial geological parameters of subsurface depths from interpolation of multiple 2-D gravity profiles with the best fit densities (Fig. 3). We first defined three surfaces with different physical properties (surface topography, a base of the basin, and top of granite intrusion) as 3-D guides for the reference model, with an original grid cell size of 270 m. Then, the initial density model of the MSB, here called a parameter reference model, has been constructed based on the representative 2-D gravity modelling interpolation results.

We use the residual CBA as subject to inverse the calculation to obtain accurate density distributions underneath the gravity stations by assigning depth parameters derived from the 3-D depth inversion as fixed parameters. The highest horizontal and vertical resolutions of Voxel density cell size that can run properly in the module are 380 and 50 m respectively. The 3-D inversion process commenced with the reference structural model construction, and then a base of the basin surface was adjusted to get the best fit solution while the other modelled parameters were kept fixed (i.e. ground and top of intrusion surfaces).

The interactive running of the VOXI module was undertaken to generate the 3-D density model and was based on the algorithm of Li and Oldenburg (1998) with prior densities from the 2-D forward modelling results (Table 2). Using the best model, i.e., the one that minimizes the data misfit, the densities were constrained by weighing of the parameter reference model and the density of each grid volume. The model was then updated through inversion. The inversion uses several iterations that are run until the difference between the gravity average of the inverted density model,

https://doi.org/10.1016/j.heliyon.2019.e01232

Table 2. The depth and density solution comparisons from a reference model (interpolation of the 2-D forward gravity) and the 3-D inversion model.

	Reference model of interpolation of the 2-D forward gravity	3-D inverse model
Maximum basin depth (m)	700	770
Density (g/cm^3)		
Granite rocks	2.64 (fixed)	2.63−2.65
Sedimentary and metasedimentary rocks	2.68 (fixed)	2.63−2.73
Sediments	2.2 (fixed)	1.93−2.32
SD[#] (mGal)	1.4	0.18

[#] Standard deviation of data error between observation and calculation gravity.

and the predicted model reached an acceptable fit, defined by less than a 5 percent (0.5 mGal) SD error. The final inversion model provides the best-fit geometry model of the subsurface layers with the highest confidence in the calculated density solutions (Blaikie et al., 2014).

4. Results

4.1. Gravity anomaly interpretation

The residual Complete Bouguer Anomaly (CBA) over the Mae Suai Basin (MSB) reveals the regions of gravity anomaly variation of -13 to 7 mGal associated with density contrasts due to different lithologies (Fig. 5). This gravity anomaly map roughly classifies features over the basin and pre-Cenozoic basements. By comparison with the geologic map (Fig. 4), gravity anomaly lows (L) correspond well to a basin locality which is associated with Cenozoic sediment units. Whereas, gravity highs (H) bound the basin to the northern, the eastern and southern margins and correspond to relatively high-density Paleozoic metasedimentary rocks. The moderate gravity anomalies (M) fit the felsic basement rock type which is compatible with the density of the Triassic granite intrusion.

The total horizontal derivative that was applied to the residual CBA represents the lateral boundary of basin anomalies and the contact boundaries of rock units. The interpreted lineament results, which are showed by largest gradient anomalies, clearly separate the basin area from the surrounding rocks at the northern, western, and eastern basin edges (Fig. 6a). These structural contact anomalies exhibit NNE-SSW, NNW-SSE, NE-SW, and NW-SE directions.

Fig. 6b illustrates Euler's depth solutions of clustered points that are located at structural contacts bounding the basin in the subsurface. The clustered depth solutions along the western margin are calculated between 300 and 500 m. The depth solutions

https://doi.org/10.1016/j.heliyon.2019.e01232

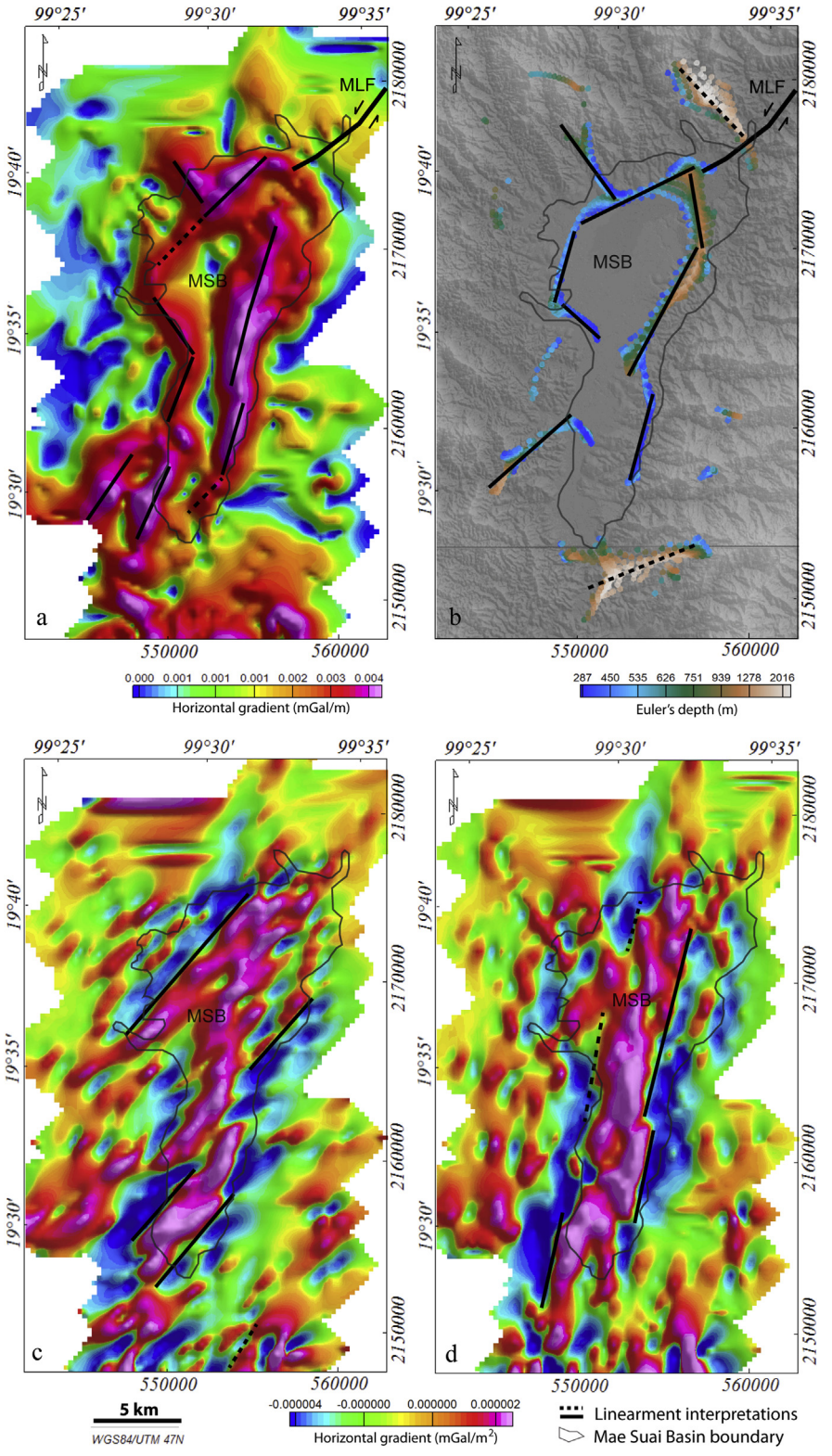

Fig. 6. Lineament interpretations displaying on a) the total horizontal derivative anomaly, b) the Euler deconvolution's cluster solutions, c) the 2nd horizontal derivative anomaly along the ESE-gradient direction (110°), and d) the 2nd horizontal derivative anomaly along the SE-gradient direction (135°). The interpretations relate to either structural faults or unconformity contacts.

https://doi.org/10.1016/j.heliyon.2019.e01232

of the northern margin yielded average depths as deep as 1000 m. The eastern margin with depths between 700 to 1300 m suggests the presence of major boundary faults as identified in a previous study (e. g. Uttamo et al., 2003a). No southern boundary fault is determined from the Euler's depth solutions.

The 2nd horizontal derivative method was applied in certain directions (SE-gradient, azimuth 135° and ESE-gradient, azimuth 100°) that are perpendicular to the expected fault strikes. The total horizontal derivative solutions can enhance the gravity gradients along straight trending lineaments (Fig. 6a). The 2nd horizontal derivative map along the SE-gradient interprets two main fault striking systems that trend NE-SW and lie at the northern and southern margins of the basin (Fig. 6c). The structural interpretation of zero-trending lineaments represents faults following the orientation of the mapped ENE-WSW trending strike-slip fault (Uttamo et al., 2003b). The 2nd horizontal derivative along the ESE-gradient enhances the fault contact interpretations along the straight, NNE-SSW oriented lineaments at the eastern and western basin margins (Fig. 6d). The basin boundary faults with a dominant normal-slip displacement may relate to the interpreted lineaments in the east.

A combination of qualitative gravity interpretations indicates the presence of ten structural lineaments (Fig. 7a, Lineaments F1 to F10) that corresponds to the recognized basin boundaries that may, or may not be controlled by faults. Based on relation to known major faults and geological features (Figs. 1 and 4), we suggest the Lineament F3 is the northern boundary fault, which is probably the sinistral MLF

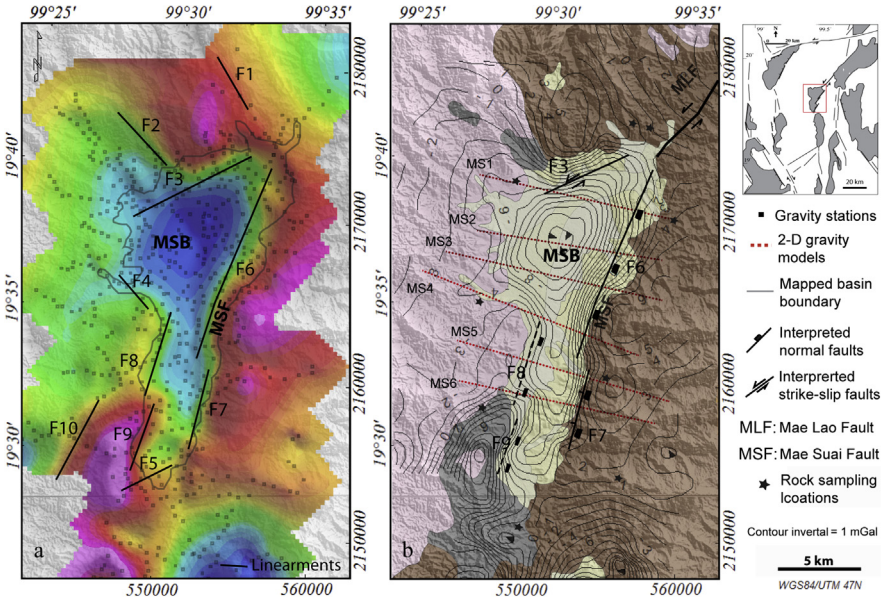

Fig. 7. a) Ten structural lineaments interpreted from integrated gravity edge detection techniques overlying the residual Complete Bouguer Anomaly (CBA). b) Possible fault interpretations and senses of movement overlying the geologic map with the residual CBA contour patterns. Red dashed lines are the 2-D forward gravity modelling profiles.

https://doi.org/10.1016/j.heliyon.2019.e01232

(Uttamo et al., 2003b; Fig. 1). The Lineaments F6 and F7 to the east are probably related to the normal-slip MSF that controls the basin expansion (Khamphira, 2016; Uttamo et al., 2003b; Fig. 1). The Lineaments F2, F4, and F10 mark unconformity contacts between basin sediments and pre-Cenozoic basement rocks (Barr et al., 1990; Fig. 7).

The basin depth interpretation from radial spectrum analysis shows the highest decay rate (Slope S1) that mark the low wavenumber of gravity signals, from a very deep source exceeding 1000 m depth in basement rocks (Fig. 8). Slope S2 represents a signal source from basin sediments at depths less than 900 m. The flatted slope of S3 of the high wavenumber is representative of gravity signals from shallow sources (<100 m deep) or disrupted surface noise from data acquisition processes. Furthermore, the calculated depth solutions of the Pdepth method represent clustered points of depth to basement contacts along these pseudo-geological models (Fig. 9). The solution clusters at the eastern contact at a depth of 1200 m may be the result of major fault controls and its synthetic faults. The solutions at the western contact are more scatted at about 500−1000 m (Fig. 9), which would be antithetic faults. Also, the Pdepth solutions clustered within the density units may indicate a heterogeneous body or complexity of paleo-geological structures.

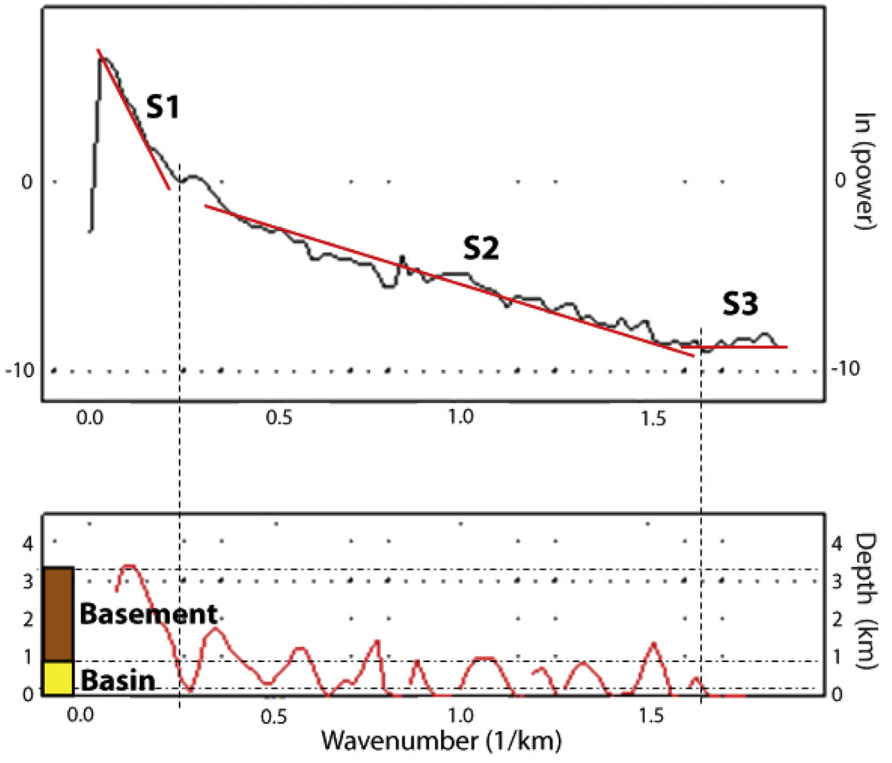

Fig. 8. Depths of gravity source solution (solid red lines) in km derived from the spectrum and slope analysis and three gravity sources from deep (slope S1), shallow (slope S2), and near-surface (slope S3).

https://doi.org/10.1016/j.heliyon.2019.e01232

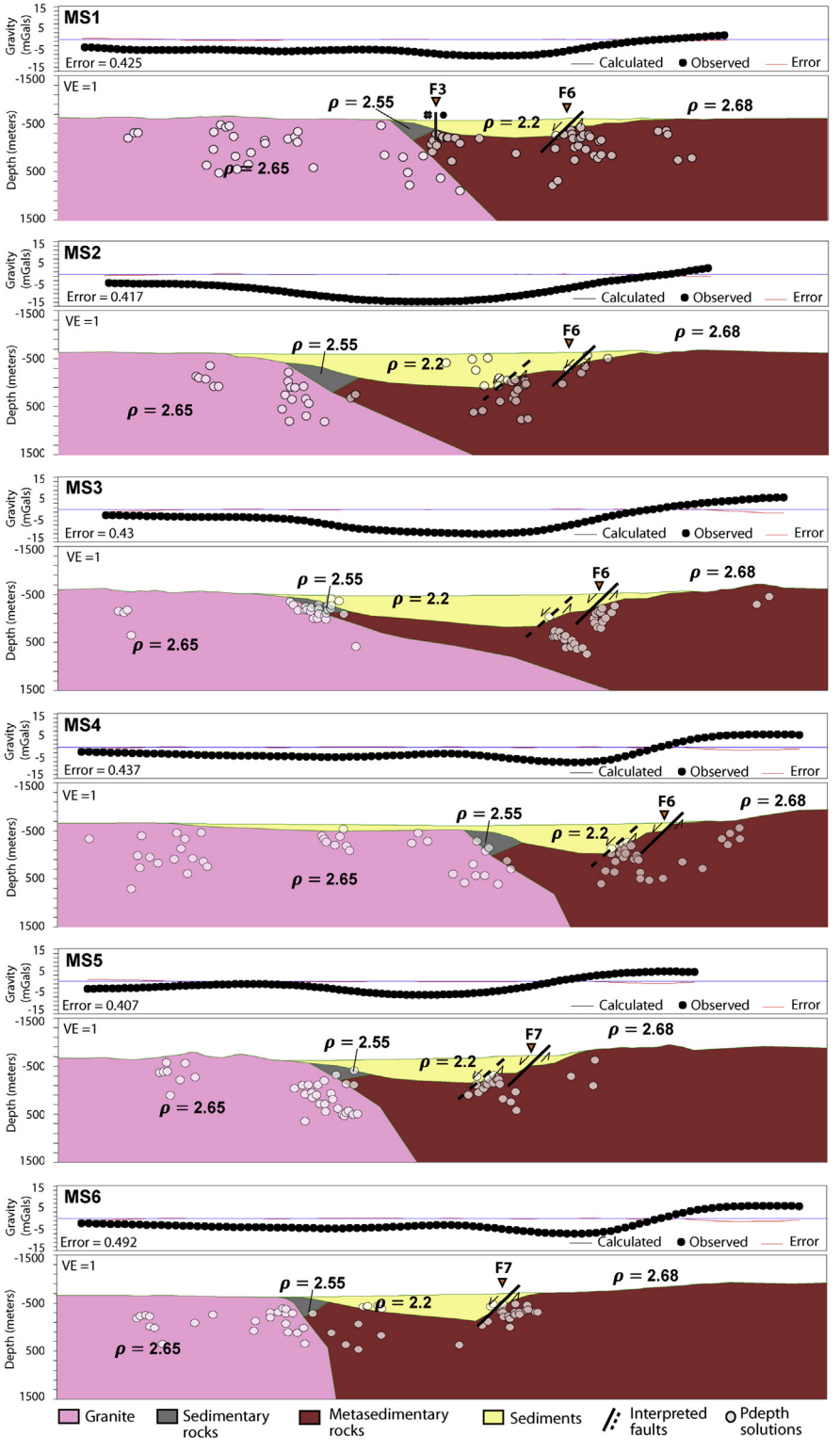

Fig. 9. Six 2-D forward gravity profiles represent a half-graben geometry with the maximum basin depth of about 700 m. Profile locations are shown in Fig. 7b. Density constraints are given in Table 1. Fault interpretations are based on gravity anomaly interpretation and analysis. White circles are depth estimations of the Pdepth method.

https://doi.org/10.1016/j.heliyon.2019.e01232

4.2. The 2-D forward models of gravity data

The 2-D forward models from gravity data produce the representative subsurface geometry of the MSB that suggest the MSB exhibits a maximum basin depth of about 700 m on the central profiles of Profiles MS2 and MS3 and less to about 600 m on the northern profiles (Fig. 7, MS1) and southern profiles (Fig. 7, MS5; MS6). Regarding surface geology constraints, the basin is bounded by metasedimentary, sedimentary, granite intrusion of the basement along the eastern, western, westernmost boundaries, respectively (Fig. 9). The steep eastern basin boundary is locally controlled by major west-dipping faults (F6; F7) and a probably synthetic fault. The smaller antithetic faults were modelled in the western boundary. Regarding basin depth and geometry, our interpretations of the MSB models seem to be reasonable and is associated with the well-known Cenozoic basins that have been investigated previously, for example, the Li Basin (DMR, 2001; Morley et al., 2000) and the Mae Moh Basin (Morley and Racey, 2011).

A Silurian-Devonian metasedimentary unit is modelled as the main lithologic basement rock unit underlying the basin unit with the thickness greater than 1500 meter. A small block of the Carboniferous sedimentary rock unit is constructed as either an

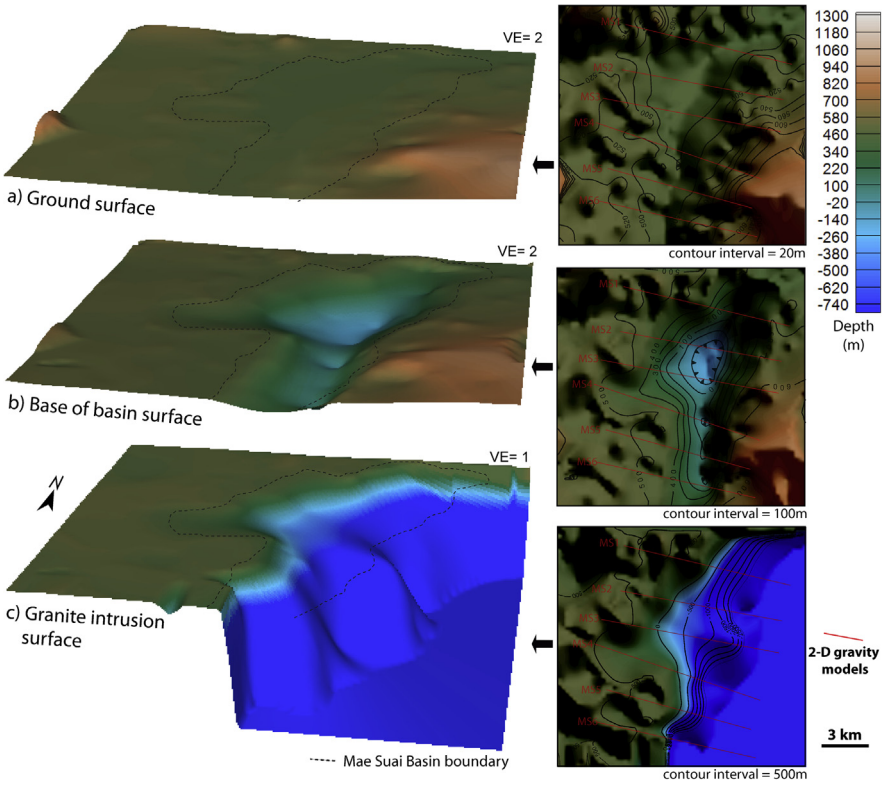

Fig. 10. Three structural surfaces were compiled in the 3-D perspective view from interpolation of the 2-D geologic profiles including 1) ground, 2) base of the basin, and 3) top of granite intrusion surfaces.

https://doi.org/10.1016/j.heliyon.2019.e01232

unconformable layer or low-angled structural contact resting on the older Silurian-Devonian unit (Barr et al., 1990; Hara et al., 2017). The younger Triassic granite pluton with unconstrained shaped crosscuts the two older basement units to the west of the basin.

4.3. The 3-D inversion models of gravity data

The 3-D geometry inversion model processed from the reference model of the 2-D gravity model interpolation (Fig. 10) exhibits the structural surface of the base of MSB with a maximum depth of around 770 m (Fig. 11b). The basin depocentre is modelled near the eastern boundary of the basin. The basin geometry is wider in

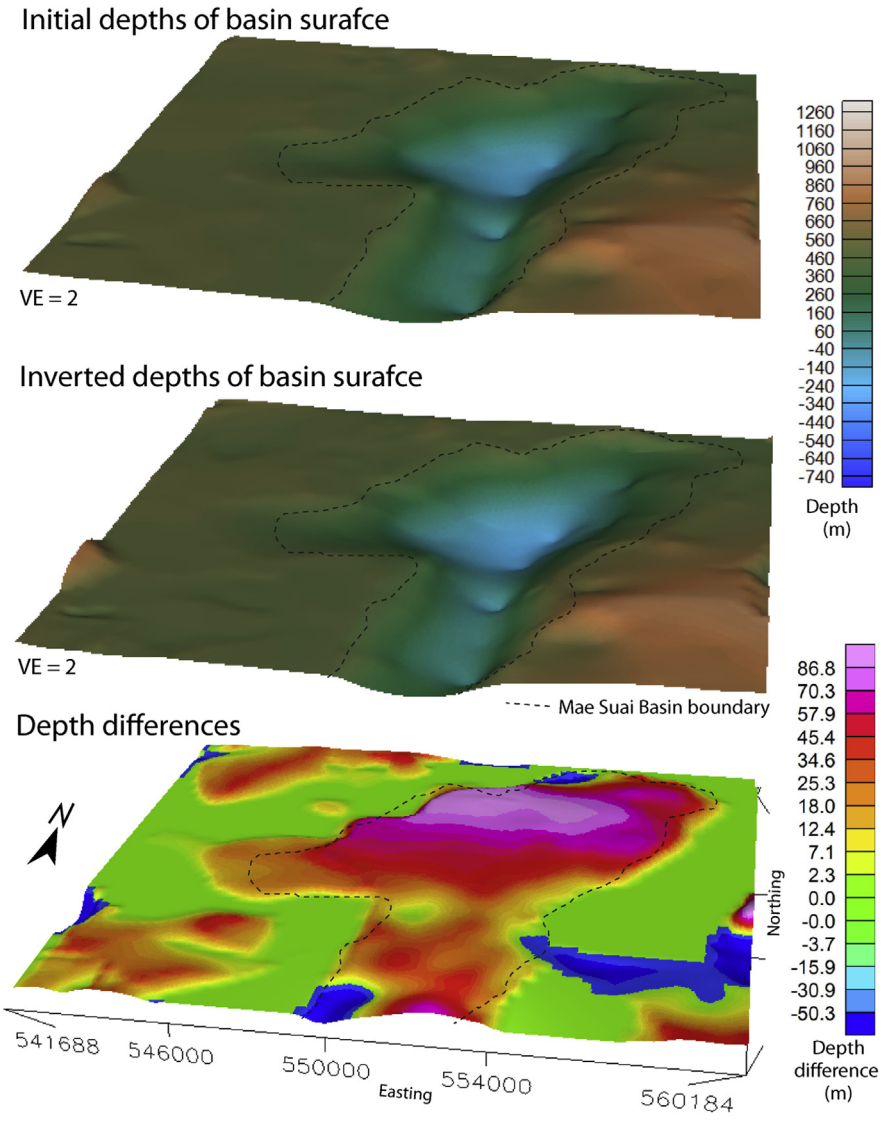

Fig. 11. Illustration of difference in structural basin surface between the initial and inverted model. The depth difference in m between initial and inverted models was shown on the lowest part.

https://doi.org/10.1016/j.heliyon.2019.e01232

the northern part and narrows to the south. The greater dip (>60°) of the basin margin confirms the presence of a basin boundary fault system along the eastern margin. The basin depth from the 3-D depth inversion model differs from the initial depth models by around 90 to -182 m (Fig. 11c). The most variable depth appears in the north where the basin depth could be changed from 700 (2-D model) to 770 m (3-D model).

The 3-D density inversion model displays density distribution results (Fig. 12). The entire density ranges from 1.93 to 2.74 g/cm^3 in bulk density system. The density models were divided into three ranges of lithologic units as follows: 1) basin sediment, 2) granite intrusion, and 3) metasedimentary rocks (Fig. 12, Table 2). The density of sediment fills within the basin range between 1.93 to 2.32 g/cm^3 with the maximum depth approximated as 770 m (Fig. 11b). The range of calculated densities represents a geologically realistic depositional model. The lowest density is about 1.93 g/cm^3 and is found near the eastern boundary where the depocentre is located (Fig. 12b). Densities distributions in the MSB basement rocks range widely between

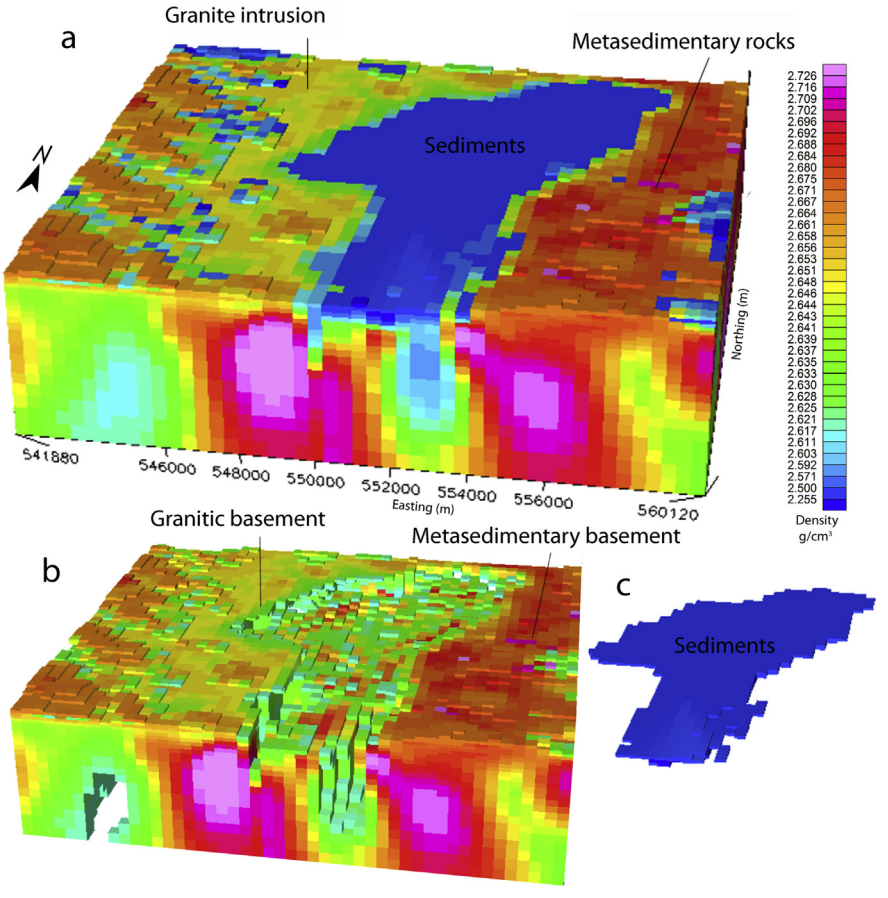

Fig. 12. The 3-D density inversion model of the Mae Suai Basin; the hot and cool colour tones represent high and low density units, respectively.

https://doi.org/10.1016/j.heliyon.2019.e01232

2.63 to 2.73 g/cm^3 (Fig. 12; Table 2). Lower density distributions between 2.63 to 2.65 g/cm^3 exhibits where the granite intrusions are modelled in the western section. The largest density ranges from 2.68 to 2.74 g/cm^3 and corresponds to metasedimentary and metasedimentary rocks in the eastern part of the basin. Low densities are observed on the eastern portion of the map representing a granite intrusion unit.

Comparison of observed and calculated gravity (Fig. 3) that results of the 3-D inversion model is the most accurate one (e. g. Skalbeck et al., 2014). The model error is revealed by the gravity data misfit between observation and calculation residual CBA data over the focused area (Fig. 13). The Standard Deviation of the optimized model error from the 3-D inversion results compared to the initial error from the 2-D forward interpolation results decreases from 1.4 to 0.18 mGal (Table 2). Such high errors on the initial model are due to the fixed density information and the interpolation method from the 2-D gravity data. A small smaller error for the 3-D inversion method indicates it gives the more accurate solution for the MSB geometry and density modelling.

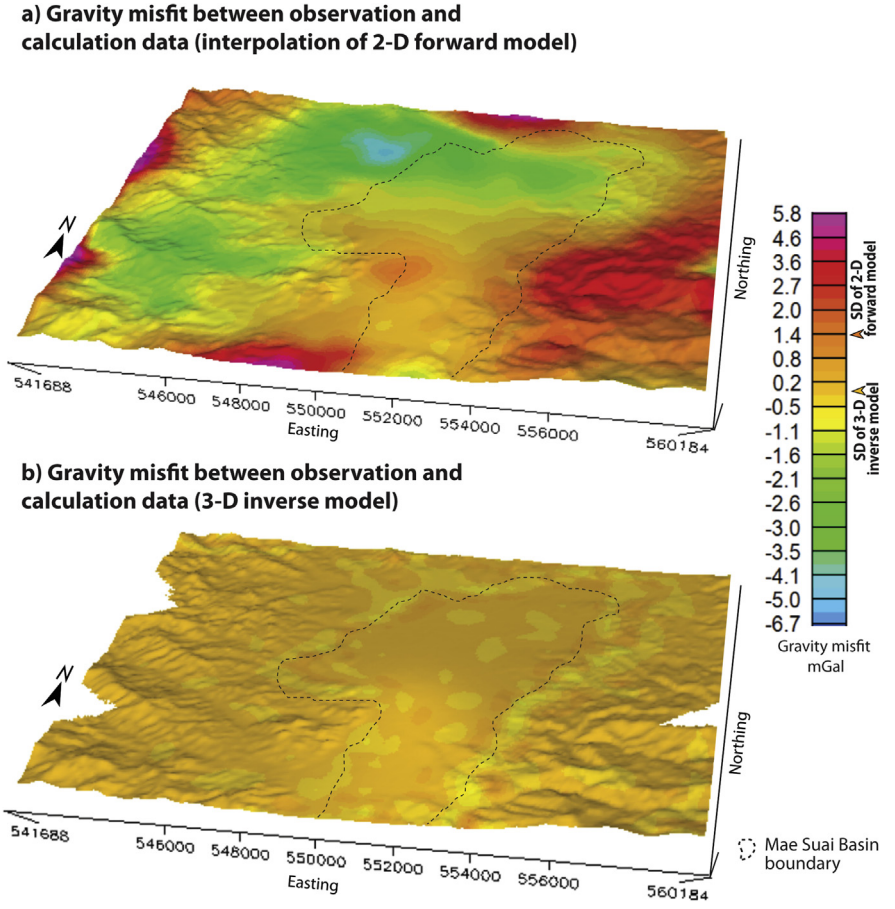

Fig. 13. Difference between observation and calculated gravity data from a) the reference model of the 2-D forward gravity interpolation and b) the 3-D inversion model.

https://doi.org/10.1016/j.heliyon.2019.e01232

5. Discussion

Quantitative interpretation of the gravity data provides an estimate of basin depth and sediment thickness. The 3-D inverted geometry of the basin model shows the Mae Suai Basin (MSB) has a maximum depth of 770 m based on the residual anomaly of the observed gravity data (Figs. 11b and 14b). The deepest area lies at the northern part of the basin and gradually decreases in thickness to the South. The basin geometry is comparable in size and geometry to well know rift basins in northern Thailand (Charusiri and Pum-Im, 2009), for example, the Li and Mae Moh Basins. The 16-km-long and 9-km-wide Mae Moh Basin is an operating lignite mine in Lampang Province, which is slightly greater in size than the MSB, and has the maximum depth to basement of 900 m (Morley and Racey, 2011). On the other hand, the smaller Li Basin has been reported to have a basin thickness of at least 750 m (DMR, 2001). Therefore, the MSB thickness based on our gravity modelling seems to be reasonable.

A pseudo-E-W geological cross-section and gravity anomaly interpretation show the MSB forms a half-graben structure controlled by the NNE-SSW striking eastern boundary fault system of the MSF (Fig. 7, F6; F7). The 2-D gravity models suggest at least two normal fault segments comprise the west-dipping normal faults of the MSF system (Fig. 14). The MSF system interpretation is also consistent with the

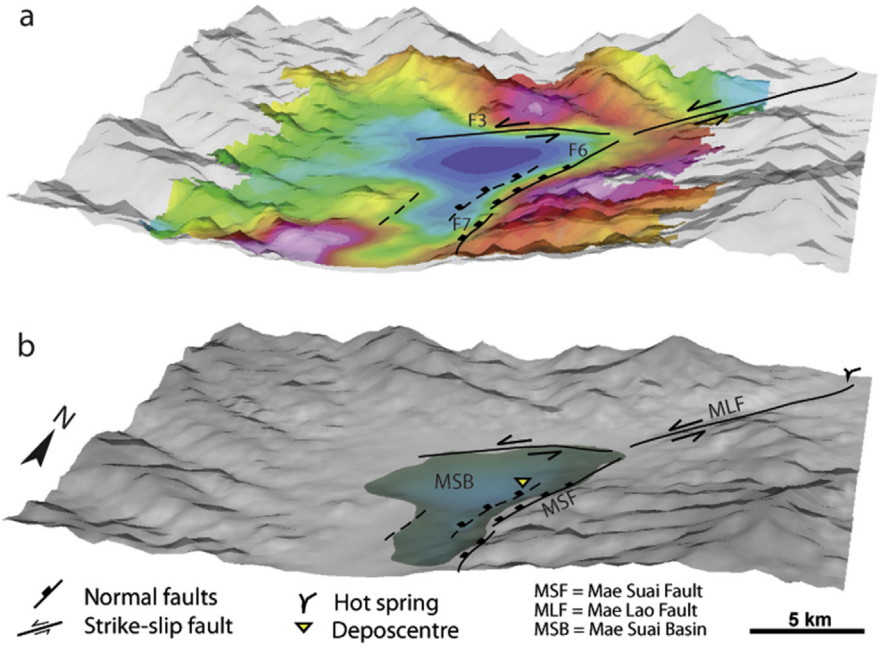

Fig. 14. a) Plausible structural scenario of fault interpretation of the 3-D depth inversion model of the Mae Suai Basin (MSB) overlaying the Digital Elevation Model map showing with the residual Complete Bouguer Anomaly map in the study area. b) The structural surface section presents the basin geometry and location of maximum depth location of the MSB and locations of fault controls.

https://doi.org/10.1016/j.heliyon.2019.e01232

structural lineaments based on Landsat satellite imagery (Khamphira, 2016). We interpret the western boundary of the basin as a nonconformity contact with the Triassic granite intrusion (Cobbing, 2011). However, these fault systems in the west need a further geological investigation to better understand structural relation between faults in the post-rift and underlying syn-rift sections associated with the basin formation (Morley, 2016).

Gravity interpretation and modelling suggest the NE-SW trending Mae Lao fault splaying into ENE-WSW (F3) and NNE-SSW (F6; MSF) trending fault segments at the NE corner of the MSB (Figs. 7b and 14). The NNE-SSW striking faults are probably a predominantly oblique-normal slip fault, while Fault F3 is probably an oblique strike-slip fault with a normal displacement component. Relocation of earthquake epicenters of the 2014 Earthquakes by Noisagool et al. (2016) and Pananont

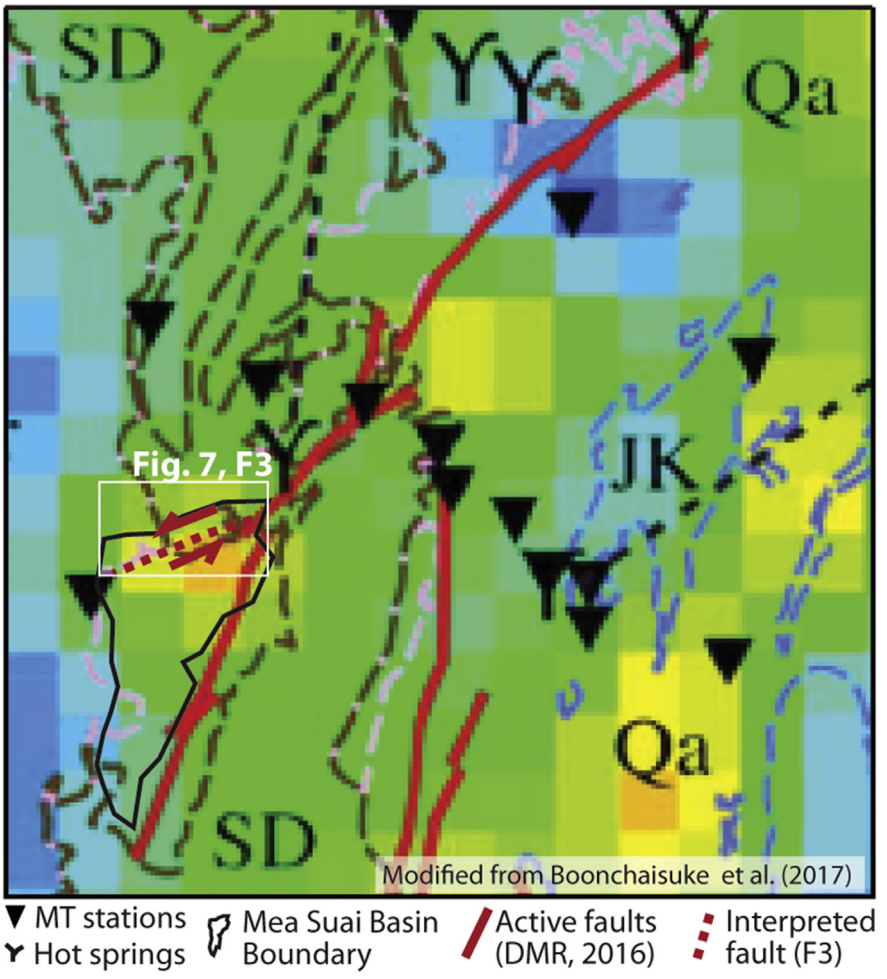

Fig. 15. Illustrating the fault F3 interpretation from gravity data corresponds well with previous studies of Magnetotellurics (MT) map from Boonchaisuk et al. (2017) that interpreted the faults on the eastern and northern parts of the Mae Suai Basin.

https://doi.org/10.1016/j.heliyon.2019.e01232

et al. (2017) (Fig. 2b) and the larger scale high conductive fault zone of the Magneto-tellurics inversion solution by Boonchaisuk et al. (2017) are also compatible with the ENE-WSE orientation of Fault F3 (Figs. 7 and 15). Interpretations of the moment tensor solutions for the 2014 earthquakes by Pananont et al. (2017) indicate Fault F3 fits with a sinistral motion model (Fig. 2b). However, the relationship between the northern segment (F3) and these previous study interpretations of the known MLF is ambiguous due to the inadequate surface evidence of a fault (Wiwegwin et al., 2015).

One typical pattern of deformation in Northern Thailand is for N-S to NNE-SSW oriented basins to be bounded at their terminations by NE-SW to ENE-WSW

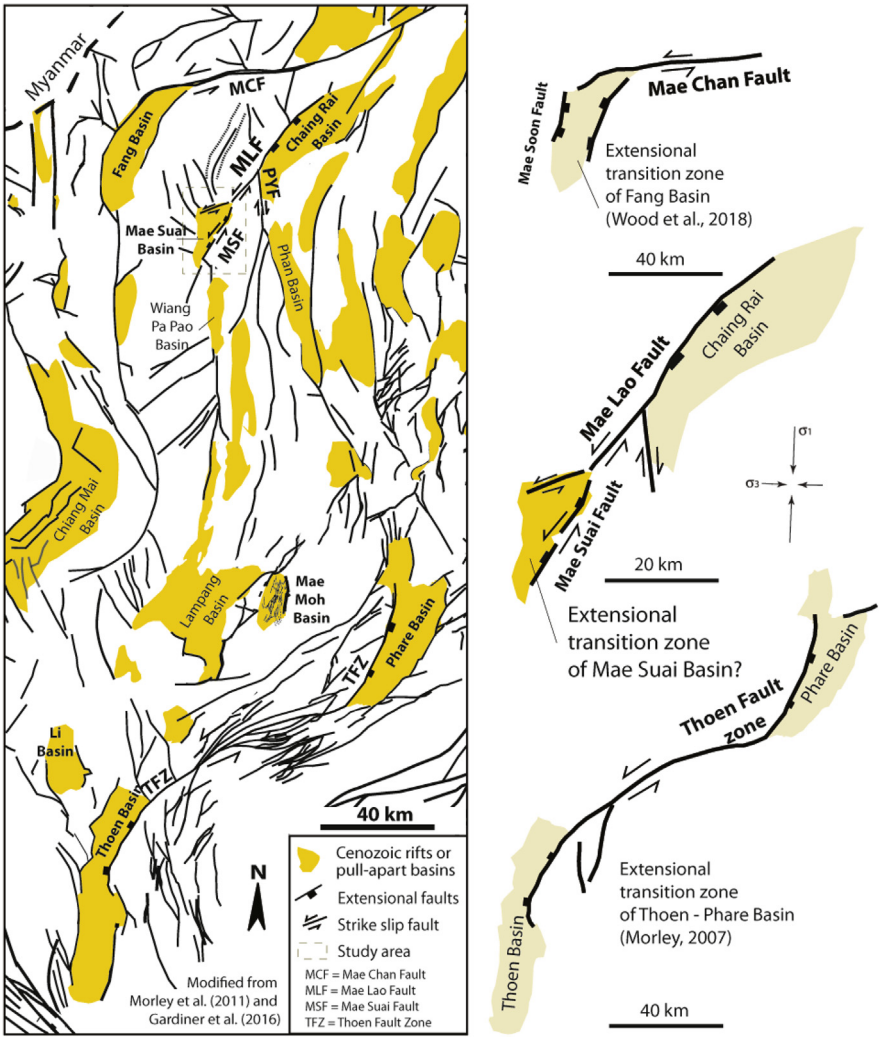

Fig. 16. Fault and basin map of Northern Thailand illustrates a mixture of Cenozoic fault orientations, where the NE-SW to N-S trending rift basin are dominant (modified from Gardiner et al., 2016; Morley et al., 2011; Morley, 2007). NE-SW to ENE-WSW fault served to link basins (e. g. the Mae Suai and Thoen Basins), and then follow an old trend in the basin. The extension direction has probably varied considerably with time but is predominately E-W to NW-SE.

https://doi.org/10.1016/j.heliyon.2019.e01232

striking faults (Fig. 1; Morley, 2007). The structural interpretations of NE-SW and NNE SSW fault zones bounding the MSB fits that pattern. An excellent example of this pattern is the Thoen Fault Zone where NE-SW oblique-slip faults link the extensional Thoen and Phrae Basins with the main segments of normal faulting run parallel to the eastern boundary of the basins (Fig. 16). The Thoen Fault has a recent history of activity, and both geomorphology and trenching across the fault zone have shown it to be extensional (Fenton et al., 1997, 2003; Pailoplee et al., 2009). Geomorphology, outcrop evidence, and seismic reflection data from the Thoen Fault Zone indicate that displacement along the NE-SW to ENE-WSW striking fault zones has been predominantly extensional (Wiwegwin et al., 2011). However, the observation by Wiwegwin et al. (2011) is from the part of the fault zone that is expected to be more extensional in character. The nature of the parts of the fault zone that, from satellite images have a stronger strike-slip character (i. e. straight, narrow fault zone, no associated basin, passing eastwards into horsetail splays), is lacking outcrop observations, any strike-slip component of motion during extension would have been sinistral (Fig. 16; Morley, 2007). Further north the similarly oriented ENE-WNW Mae Chan Fault is a sub-vertical sinistral strike-slip fault (Wood et al., 2018).

6. Conclusions

We provide pseudo-geological models of the subsurface geometry of the Mae Suai Basin (MSB) and related fault structures that were created based on new gravity anomaly data analysis and 2-D and 3-D gravity modelling with constraints from surface geology and seismological information. The MSB is an extensional half graben, with the main extension faults on the eastern margin of the basin. The gravity modelling indicates the maximum basin depth is approximately 770 m, similar to the Li Basins. Densities of the basin materials range between 1.9 - 2.3 g/cm^3 are reasonable when compared to other Tertiary basins such as the Chiang Mai Basin. The basin boundary and fault locations corresponded well with previous studies that identified bounding faults on the northern, southern, and eastern parts of MSB. The NE-SW trending strike-slip faults along the northern margin of the basin correspond to the Mae Lao Fault orientation. A similarly trending strike-slip fault zone is interpreted on the southern margin. The eastern margin is dominated by a NNE-trending normal fault system related to the Mae Suai Fault. The MSB has an extensional half-graben structure where the major NNE-trending Mae Suai Fault bounds the eastern margin. Consequently, the basin formation can be interpreted to form an extensional transfer zone where the sinistral strike-slip faults at the northeastern margins link with the normal faults system at the eastern margin. The structural pattern is similar to the typical N-S to NNE-SSW oriented basins dominantly controlled by NE-SW to ENE-SWS trending faults in Northern Thailand which include the examples of the Thoen and Phrae Basins and the Fang Basin-Mae Chan Fault.

https://doi.org/10.1016/j.heliyon.2019.e01232

Declarations

Author contribution statement

Niti Mankhemthong, Suebchart Kanthiya: Conceived and designed the experiments; Performed the experiments; Analyzed and interpreted the data; Contributed reagents, materials, analysis tools or data; Wrote the paper.

Christopher Morley: Analyzed and interpreted the data.

Funding statement

This work was supported by the Development and Promotion of Science and Technology Graduate with First Placement research fund, Chiang Mai University Graduated Research scholarships and the Geophysics Research Laboratory at Department of Geological Sciences, Chiang Mai University.

Competing interest statement

The authors declare no conflict of interest.

Additional information

Supplementary content related to this article has been published online at https://doi.org/10.1016/j.heliyon.2019.e01232.

Acknowledgements

We are grateful to Siriporn Chaisri, Dhiti Tulyatid, and Songkhun Boonchaisuk for discussions related to geophysical and geological backgrounds. We hugely thank for Adul Yawichai, Thanavut Minin, and Chanin Sangthip for supporting all of gravity data acquisition. We would like to thank anonymous reviewers for helpful comments that improved the manuscript and for editorial help. We acknowledge the Geophysics Research Laboratory at the Department of Geological Sciences, Chiang Mai University, for providing a gravity meter and differential GPS system and processing software of gravity and GPS data.

References

Barr, S.M., Tantisukrit, C., Yaowanoiyothin, W., Macdonald, A.S., 1990. Petrology and tectonic implications of Upper Paleozoic volcanic rocks of the Chiang Mai belt, northern Thailand. J. Southeast Asian Earth Sci. 4, 37−47.

Blaikie, T.N., Ailleres, L., Betts, P.G., Cas, R.A.F., 2014. Interpreting subsurface volcanic structures using geologically constrained 3-D gravity inversions: examples

of maar-diatremes, Newer Volcanics Province, southeastern Australia. J. Geophys. Res. Solid Earth 119, 3857–3878.

Boonchaisuk, S., Noisagool, S., Amatyakulb, P., Rung-Arunwan, T., Vachiratienchaic, C., Siripunvaraporn, W., 2017. 3-D magnetotelluric imaging of the Phayao Fault Zone, Northern Thailand: evidence for saline fluid in the source region of the 2014 Chiang Rai earthquake. J. Asian Earth Sci. 147, 210–221.

Bunopas, S., 1981. Paleogeographic History of Western Thailand and Adjacent Parts of Southeast Asia-A Plate Tectonics Interpretation. Victoria University of Willington, (unpublished Ph.D. thesis), reprinted 1982 as Geological Survey Paper no.5. Geological Survey Division, Department of Mineral Resources, Bangkok.

Charusiri, P., Pum-Im, S., 2009. Cenozoic tectonic evolution of major sedimentary basin in Central, Northern, and the Gulf of Thailand. Bull. Earth Sci. Thail. 2, 40–62.

Cobbing, E.J., 2011. Granitic rocks. In: Ridd, M.F., Barber, A.J., Crow, M.J. (Eds.), The Geology of Thailand. Geological Society, London, pp. 441–458.

Department of Groundwater Resources, 2009. Potential Groundwater Potential Assessment Project (Chiang Rai - Phayao). Department of Groundwater Resources, Bangkok (in Thai).

Department of Mineral Resources, 2001. Geology of Thailand. Department of Mineral Resources, Bangkok (in Thai).

Department of Mineral Resources, 2007. North Geological Maps by Province. http://www.dmr.go.th/download/pdf/North/Chiangrai.pdf. (Accessed 1 August 2017).

Department of Mineral Resources, 2014. Report of Geophysical Survey in Active Fault Area at Chiang Rai Province, 5th May 2014. Department of Mineral Resources, Bangkok (in Thai).

Department of Mineral Resources, 2016. Active Fault Map of Thailand. http://www.dmr.go.th. (Accessed 1 August 2017).

Fenton, C.H., Charusiri, P., Hinthong, C., Lumjuan, A., Mangkonkarn, B., 1997. Late Quaternary faulting in northern Thailand. In: The International Conference on Stratigraphy and Tectonic Evolution of SE Asia and South Pacific, Bangkok, Department of Mineral Resources, August 19–24, pp. 436–452.

Fenton, C.H., Charusiri, P., Wood, S.H., 2003. Recent paleoseismic investigations in northern and western Thailand. Ann. Geophys. 46, 957–981.

Gardiner, N.J., Roberts, N.M.W., Morley, C.K., Searle, M.P., Whitehouse, M.J., 2016. Did Oligocene crustal thickening precede basin development in northern

 https://doi.org/10.1016/j.heliyon.2019.e01232

Thailand? A geochronological reassessment of Doi Inthanon and Doi Suthep. Lithos 240-243, 69–83.

Hara, H., Kunii, M., Miyake, Y., Hisada, K., Kamata, Y., Ueno, K., Kon, Y., Kurihara, T., Ueda, H., Assavapatchara, S., Treerotchananon, A., Charoentitirat, T., Charusiri, P., 2017. Sandstone provenance and U–Pb ages of detrital zircons from Permian–Triassic forearc sediments within the Sukhothai Arc, northern Thailand: record of volcanic-arc evolution in response to Paleo-Tethys subduction. J. Asian Earth Sci. 146, 30–55.

Hinze, J.W., Vonfrese, R.R.B., Saad, A.H., 2012. Gravity and Magnetic Exploration-Principles, Practice and Applications. Cambridge University Press, Cambridge, UK, 512p.

Kearey, P., Brooks, M., Hill, I., 2002. An Introduction to Geophysical Exploration, third ed. Blackwell Publishing, Oxford.

Khamphira, C., 2016. Geomorphologic and Earthquake Evidence for Faulting in Wiang Pa Pao – Mae Suai Basin, Chiang Rai Province. Bachelor thesis. Chiang Mai University, 68p (in Thai).

Lacassin, R., Maluski, H., Leloup, P.H., Tapponnier, P., Hinthong, C., Siribahakdi, K., Chuaviroj, S., Charoenravat, A., 1997. Tertiary diachronic extrusion and deformation of western Indochina: structural and 40Ar/39Ar evidence from NW Thailand. J. Geophys. Res. 102, 10013–10037.

Li, Y., Oldenburg, D.W., 1998. 3-D inversion of gravity data. Geophysics 63, 109–119.

McLean, M.A., Rawling, T.J., Betts, P.G., Phillips, G., Wilson, C.J.L., 2008. Three-dimensional inversion modelling of a Neoproterozoic basin in the southern Prince Charles mountains, east Antarctica. Tectonophysics 456, 180–193.

Milsom, J., 2011. Regional Geophysics. In: Ridd, M.F., Barber, A.J., Crow, M.J. (Eds.), The Geology of Thailand. Geological Society, London, pp. 493–506.

Morley, C.K., 2001. Combined escape tectonics and subduction rollback-back arc extension: a model for the evolution of Cenozoic rift basins in Thailand, Malaysia and Laos. J. Geol. Soc. Lond. 158, 461–474.

Morley, C.K., 2007. Variations in Late Cenozoic-Recent strike-slip and oblique-extensional geometries, within Indochina: the influence of pre-existing fabrics. J. Struct. Geol. 29, 36–58.

Morley, C.K., 2009. Geometry and evolution of low-angle normal faults (LANF) within a Cenozoic high-angle rift system, Thailand: implications for sedimentology and the mechanisms of LANF development. Tectonics 28.

https://doi.org/10.1016/j.heliyon.2019.e01232

Morley, C.K., 2016. The Impact of Multiple Extension Events, Stress Rotation and Inherited Fabrics on normal Fault Geometries and Evolution in the Cenozoic Rift Basins of Thailand. Geological Society, London. Special Publications. 439.

Morley, C.K., Racey, A., 2011. Tertiary stratigraphy. In: Ridd, M.F., Barber, A.J., Crow, M.J. (Eds.), The Geology of Thailand. Geological Society, London, pp. 223–271.

Morley, C.K., Charusisri, P., Wantkinson, I.M., 2011. Structural geology of Thailand during the Cenozoic. In: Ridd, M.F., Barber, A.J., Crow, M.J. (Eds.), The Geology of Thailand. Geological Society, London, pp. 273–333.

Morley, C.K., Sangkumarn, N., Hoon, T.B., Chonglakmani, C., Lambiase, J., 2000. Structural evolution of the Li basin, northern Thailand. J. Geol. Soc. 157, 483–492.

Nabighian, M.N., 1972. The analytic signal of two-dimensional magnetic bodies with polygonal cross-section: its properties and use for automated anomaly interpretation. Geophysics 37, 507–517.

Noisagool, S., Boonchaisuk, S., Pronsopin, P., Siripunvaraporn, W., 2016. The regional moment tensor of the 5 May 2014 Chiang Rai earthquake (Mw = 6.5), Northern Thailand, with its aftershocks and its implication to the stress and the instability of the Phayao Fault Zone. J. Asian Earth Sci. 127, 231–245.

Pailoplee, S., Sugiyama, Y., Charusiri, P., 2009. Deterministic and probabilistic seismic hazard analyses in Thailand and adjacent areas using active fault data. Earth Planets Space 61, 1313–1325.

Pananont, P., Herman, M.W., Pornsopin, P., Furlong, K.P., Habangkaem, S., Waldhauser, F., Wongwai, W., Limpisawad, S., Warnitchai, P., Kosuwa, S., Wechbunthung, B., 2017. Seismotectonics of the 2014 Chiang Rai, Thailand, earthquake sequence. J. Geophys. Res. Solid Earth 122, 6367–6388.

Piyasin, S., 1972. Geology of the Changwat Lumpang Sheet NE 47-7, Scale 1: 250000. Report of Investigation, No. 14. Department of Mineral Resources, Bangkok (in Thai).

Reid, A.B., Allsop, J.M., Granser, H., Millet, A.J., Somerton, I.W., 1990. Magnetic interpretation in three dimensions using Euler deconvolution. Geophysics 55, 8–91.

Rhodes, B.R., Perez, R., Lamjuan, A., Kosuwan, S., 2003. Kinematics and tectonic implications of the Mae Kuang fault, northern Thailand. J. Asian Earth Sci. 24, 79–89.

Robinson, E.S., Crouch, C., 1998. Basic Exploration Geophysics. John Wiley & Sons, New York.

https://doi.org/10.1016/j.heliyon.2019.e01232

Skalbeck, J.D., Koski, A.J., Peterson, M.T., 2014. Estimation of Precambrian basement topography in Central and Southeastern Wisconsin from 3D modelling of gravity and aeromagnetic data. J. Appl. Geophys. 106, 187−195.

Spector, A., Grant, F., 1970. Statistical models for interpreting aeromagnetic data. Geophysics 35, 293−302.

Talwani, M., Heirtzler, J.R., 1964. Computation of gravity anomalies caused by two dimensional structures of arbitrary shapes. Geol. Sci. 9, 464−480.

Talwani, M.J., Worazel, J.L., Landisman, M., 1959. Rapid gravity computations for two-dimensional bodies with application to the Mendocino submarine fracture zone. J. Geophys. Res. 64, 49−59.

Telford, W.M., Geldart, L.P., Sheriff, R.E., 1990. Applied Geophysics. Cambridge University Press, New York.

Thurston, J.B., Smith, R.S., 1997. Automatic conversion of magnetic data to depth, dip, and susceptibility contrast using the SPI (TM) method. Geophysics 62, 807−813.

Uttamo, W., Elders, C., Nichols, G., 2003a. Relationships between Cenozoic strike-slip faulting and basin opening in northern Thailand. In: Storti, F., Holdsworth, R.E., Salvini, F. (Eds.), Intraplate Strike-Slip Deformation Belts. Geological Society, London, Special Publications, pp. 89−108.

Uttamo, W., Singharajwarapan, S., Kantaroj, W., Chantarapaserd, S., 2003b. Tectonic Settings and mineral Deposits at Mae Suai-Wiang Pa Pao Area, Northern Thailand. Chiang Mai University (in Thai).

U.S. Geological Survey, 2014. M 6.1 - 13km NNW of Phan, Thailand. http://earthquake. usgs.gov/earthquakes/eventpage/usb000qack#shakemap. (Accessed 1 August 2017).

Wattananikorn, K., Beshir, J.A., Nochaiwong, A., 1995. Gravity interpretation of Chiang Mai basin, northern Thailand: concentrating on ban Thung Sieo area. Southeast Asian Earth Sci. 12 (1−2), 53−64.

Whitehead, N., Musselman, C., 2006. Montaj Gravity and Terrain Correction, Gravity Data Processing Extension for Oasis Montaj v6.3. Tutorial and User Guide Geosoft Inc., Toronto. Unpublished document.

Wiwegwin, W., Kosuwan, S., Limpiswat, S., Saithong, P., Pananont, P., 2015. The biggest earthquake of the century in Thailand: ML6.1 Mae Lao earthquake, Chiang Rai Province. J. Geol. Soc. Thai. 1, 1−11.

https://doi.org/10.1016/j.heliyon.2019.e01232

Wiwegwin, W., Sugiyama, Y., Hisada, K., Charusiri, P., 2011. Re-evaluation of the activity of the Thoen Fault in the Lampang Basin, northern Thailand, based on geomorphology and geochronology. Earth Planets Space 63, 975–990.

Wongwanich, T., Boucot, A.J., 2011. Devonian. In: Ridd, M.F., Barber, A.J., Crow, M.J. (Eds.), The Geology of Thailand. Geological Society of London, pp. 53–70.

Wood, S.H., Kaewsomwang, P., Singharajwarapan, F.S., 2018. Geologic framework of the Fang Hot Springs area with emphasis on structure, hydrology, and geothermal development, Chiang Mai Province, Northern Thailand. Geotherm. Energy 6, 51.

https://doi.org/10.1016/j.heliyon.2019.e01232